Check for updates

Chemistry
A European
Journal

Chemistry Europe
European Chemical Societies Publishing

Accepted Article

Title: Towards Photochromic Azobenzene-Based Inhibitors for Tryptophan Synthase

Authors: Nadja A. Simeth, Thomas Kinateder, Chitra Rajendran, Julian Nazet, Rainer Merkl, Reinhard Sterner, Burkhard König, and Andrea Christa Kneuttinger

This manuscript has been accepted after peer review and appears as an Accepted Article online prior to editing, proofing, and formal publication of the final Version of Record (VoR). This work is currently citable by using the Digital Object Identifier (DOI) given below. The VoR will be published online in Early View as soon as possible and may be different to this Accepted Article as a result of editing. Readers should obtain the VoR from the journal website shown below when it is published to ensure accuracy of information. The authors are responsible for the content of this Accepted Article.

To be cited as: *Chem. Eur. J.* 10.1002/chem.202004061

Link to VoR: https://doi.org/10.1002/chem.202004061

WILEY-VCH

10.1002/chem.202004061

WILEY-VCH

FULL PAPER

Towards Photochromic Azobenzene-Based Inhibitors for Tryptophan Synthase

Nadja A. Simeth,[a], [b], ‡, * Thomas Kinateder,[c], ‡ Chitra Rajendran,[c] Julian Nazet,[c] Rainer Merkl,[c] Reinhard Sterner,[c] Burkhard König[a], and Andrea C. Kneuttinger[c]*

[a] Dr. N. A. Simeth, Prof. Dr. B. König
Institute for Organic Chemistry, Department of Chemistry and Pharmacy
University of Regensburg
Universitätsstraße 31, 93040 Regensburg, Germany.
[b] Dr. N. A. Simeth
Stratingh Institute for Chemistry, Faculty of Science and Engineering
University of Groningen
Nijenborgh 4, 9747 AG Groningen, The Netherlands.
[c] T. Kinateder, Dr. Chitra Rajendran, J. Nazet, Prof. Dr. R. Merkl, Prof. Dr. R. Sterner, Dr. A. C. Kneuttinger
Institute for Biophysics and Physical Biochemistry
Regensburg Center for Biochemistry
University of Regensburg
Universitätsstraße 31, 93040 Regensburg, Germany.
* E-mail:andrea.kneuttinger@ur.de; n.a.simeth@rug.nl
‡ The authors contributed equally.
Supporting information for this article is given via a link at the end of the document.

Abstract: Light-regulation of drug molecules has gained growing interest in the fields of biochemical and pharmacological research in recent years. In addition, a serious need for novel molecular targets of antibiotics has emerged presently. Here, we present the development of a photo-controllable, azobenzene-based antibiotic precursor towards tryptophan synthase (TS), an essential metabolic multienzyme complex in bacteria. The compound exhibited a medium-strong inhibition of TS in its *E* configuration, and a 5-fold lower inhibition strength in its *Z* configuration. Using a combination of biochemical, crystallographic, and computational analyses we characterized the inhibition mode of this compound. Remarkably, binding of the inhibitor to a hitherto not considered cavity causes an unproductive conformation of TS leading to non-competitive inhibition of tryptophan production. In conclusion, we created a promising lead compound for the combat of bacterial diseases, which targets an essential metabolic enzyme, and whose inhibition strength can be controlled with light.

Introduction

Antibiotics are crucial for modern medicine.[1] They are used to cure bacterial illnesses and infections, and to facilitate major surgical operations. Most of us have used them at least once in our lives. To further our understanding of their mode of action, antibiotic precursors are often designed for biochemical and pharmaceutical studies. This ultimately paves the way for drugs that are highly efficient, specific and less prone towards the buildup of resistance. In particular, focusing on novel types of macromolecular targets, and innovative strategies to circumvent resistance are paramount to this cause.[2]

Most antibiotics engage in bacterial cell-division processes or weaken the bacterial membrane.[3] Recently, the search for alternative targets was expanded to metabolic enzymes,[4] such as the well-investigated multienzyme complex tryptophan synthase (TS). TS catalyzes the last two steps of tryptophan biosynthesis in bacteria, plants, and fungi.[5] The complex consists of TrpA (α) and TrpB (β), which are arranged as a heterotetramer in a linear $\alpha\beta\beta\alpha$ configuration.[6] The functional unit of TS is thereby formed by one $\alpha\beta$ heterodimer (Figure 1A).[7] Tryptophan production starts with the TrpA reaction, in which indole-3-glycerol phosphate (IGP) is cleaved in a retro-aldol reaction to glyceraldehyde 3-phosphate (GAP) and indole.[7] In the next step, indole travels through an intermolecular channel to the active site of TrpB,[8] where it is used to synthesize tryptophan from serine using pyridoxal phosphate (PLP) as a cofactor.[5b,9] Both reactions, indole synthesis in TrpA and tryptophan synthesis in TrpB, require a tight allosteric regulation of both subunits (Figure 1B).[6a,10] Upon binding of IGP in the TrpA active site, the affinity for serine in the TrpB active site is enhanced, as shown by a reduced K_M^{Ser} value, so that the initial reaction of serine with PLP to an aminoacrylate intermediate is facilitated.[8] The formation of the aminoacrylate in turn enhances the turnover of IGP to indole as manifested in an increased k_{cat} value of TrpA.[11] Structural analyses of TS from *Salmonella typhimurium* revealed that a conformational change of the communication (COMM) domain, which includes around 90 residues in TrpB, is in particular responsible for the propagation of the allosteric signals between the two active sites.[12] In the absence of IGP and serine, the COMM domain exhibits an open conformation, while binding of IGP in TrpA and the subsequent formation of aminoacrylate in TrpB induce a stepwise transition to a closed conformation.[12b,13] As mammals lack the genes for the biosynthetic pathway of tryptophan, TS represents an excellent target for the development of new antibiotics. Previous studies already reported inhibitors towards TS that either compete with IGP for the active site of TrpA,[14] bind at the TrpA:TrpB interface,[15] or interact with the hydrophobic intermolecular indole channel in TrpB.[16] These examples provide good starting points for the development of antibiotic agents.

Accepted Manuscript

This article is protected by copyright. All rights reserved.

10.1002/chem.202004061

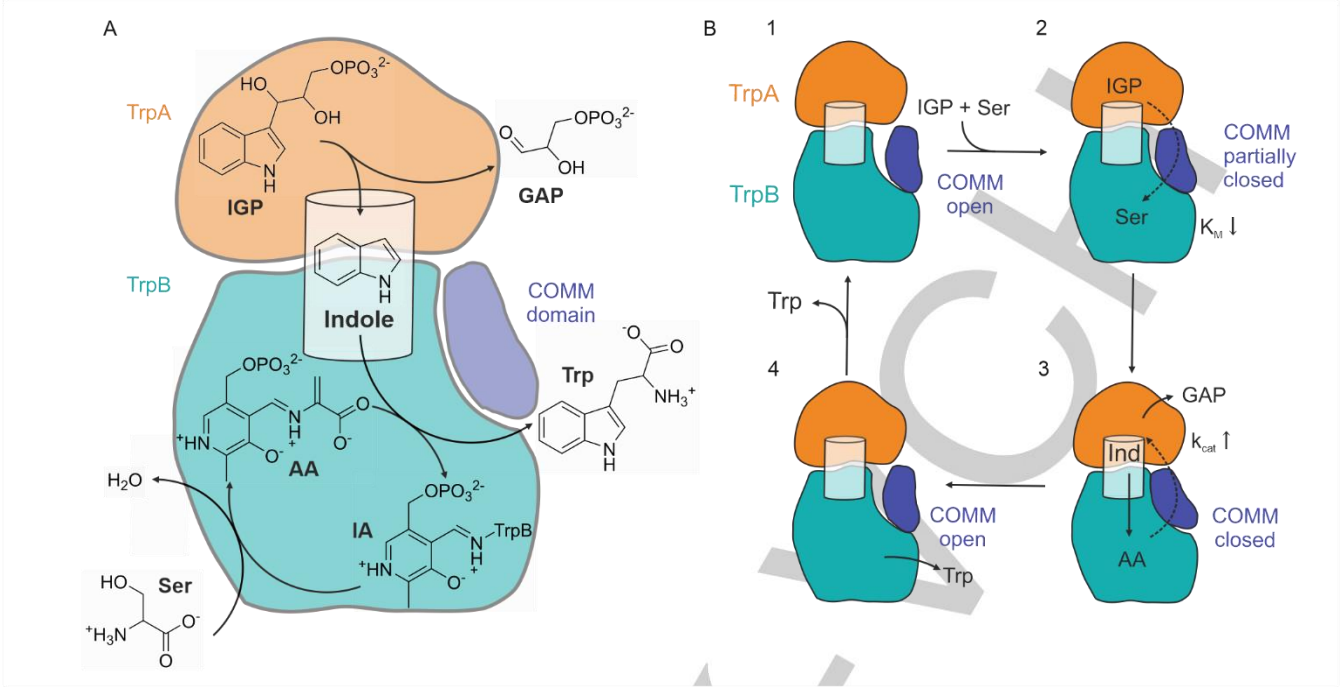

Figure 1. Schematic representation of the tryptophan synthase (TS) functional unit, its reactions and allosteric regulation. **A** In TrpA (orange) indole-3-glycerol phosphate (IGP) is cleaved into glyceraldehyde 3-phosphate (GAP) and indole, which is channeled through a hydrophobic tunnel (white) to TrpB (cyan). In TrpB, pyridoxal phosphate, bound as internal aldimine (IA), reacts with serine (Ser) to form aminoacrylate (AA), which subsequently reacts with indole to the final product tryptophan (Trp). The communication (COMM) domain of TrpB is shown in dark blue. **B** In the absence of serine and IGP, TS is inactive and the COMM domain in TrpB adopts an "open" conformation (1). Binding of IGP to the TrpA active site leads to a partial closure of the COMM domain and an allosteric activation of TrpB enhancing the binding affinity ($K_M\downarrow$) for its substrate serine (2). The formation of AA from PLP and serine in TrpB results in a fully closed COMM domain and an allosteric activation of TrpA, which increases the turnover of IGP to indole (Ind) and GAP ($k_{cat}\uparrow$, 3). Finally, Trp, the reaction product of AA and Ind, dissociates from TrpB, and the COMM domain returns to its inactive "open" conformation (4).[13c]

Direct control of the efficacy of drugs is an innovative approach in biochemical and pharmacological studies, which is increasingly used to gain in depth knowledge of the mode of action. Temporally resolved activation allows one to unambiguously associate the observed effect to the drug. Most recently, the spatio-temporal control of drugs has been addressed by developing light-responsive, bioactive molecules in the growing field of *photopharmacology*.[17] Besides many other applications, such as photo-sensitive proteins,[18] DNA modulators,[19] kinase inhibitors,[20] and PROTACs,[21] the first photo-controllable antibiotics have been developed.[22] The principle of *photopharmacology* is based on a seemingly simple strategy; the designed drug consists of moieties that convey a biological response, such as an inhibitory effect toward the target structure, and a photo-responsive part that facilitates a light-induced structural change. By this, the drug is rendered effective in one configuration and ineffective in the other. Moreover, the different photoisomers can exhibit different pharmacokinetic and pharmacodynamic properties. A frequently used photo-actuator is azobenzene, a molecule consisting of two aryl units connected by a diazo bond (N=N). Upon irradiation with light of a specific wavelength, the thermodynamically more stable *E* isomer can be converted into its corresponding *Z* form. This configurational change affects several properties of the molecule including its UV-visible absorption spectrum, its steric demand, its polarity and, if embedded in a suitable bioactive structure, its affinity towards e.g. enzymes. The metastable *Z* isomer can be converted back into the *E* form either by irradiation with light of lower energy or thermally.[23]

In recent years, our groups pioneered the control of metabolic multienzyme complexes with diverse photo-responsive tools.[24] In the present work, we intend to explore photo-controllable inhibitors for the essential multienzyme complex TS of the enteric human pathogen *S. typhimurium*[25] as potential antibiotic structures. We will discuss the design and synthesis of a small library of azobenzene-based compounds, investigate their photochemical behavior and thoroughly study their mode of inhibition towards TS. Finally, we will substantiate these findings with crystallographic and computational methods and outline a mode of action for this potential drug precursor.

Results and Discussion

Design and Molecular Realization. Previous studies have described various target sites for inhibitors in the TS complex.[14b,14c,15,16] We reasoned that targeting the TrpA active site is a good starting point for the design of a photo-controllable inhibitor. Hence, we analyzed the crystal structures of TS with IGP or the inhibitor indole-3-propanol phosphate bound to TrpA[6c,12a] to identify the most important ligand-enzyme interactions and steric requirements for binding to the active site (Figure S1.1.). Since both ligands form strong hydrogen bonds to residues in the active site with their phosphate motif and their *N*H moiety

This article is protected by copyright. All rights reserved.

Accepted Manuscript

10.1002/chem.202004061

(Figure 2A), we integrated these two groups into our inhibitor design.

Consequently, our synthetic ligands consist of a phosphate motif, to which an *N*H containing amide moiety is attached via an alkyl linker (Figure 2B). To allow for reversible photo-switching, we chose to extend the binding part of the molecule with an azobenzene-photoswitch attached to the carbonyl group.[26] Finally, we varied the length of the alkyl or aryl linker to find an inhibitor, which exhibits the optimal geometry to bind to the TrpA active site in one but not in the other photoisomer. Furthermore, we hypothesized that the *E* isomers would show stronger binding, whereas the increased steric demand in the *Z* isomers should lead to weaker binding. Following this assumption, the inhibitors in *E* should competitively displace IGP, and inhibit the TrpA reaction, while the *Z* isomer should allow for IGP binding and turnover. As a result, due to the strong dependence of the TrpB reaction on binding of IGP to the TrpA active site, we would be able to simultaneously control IGP turnover in TrpA, and tryptophan production in TrpB with light (Figure 2C).

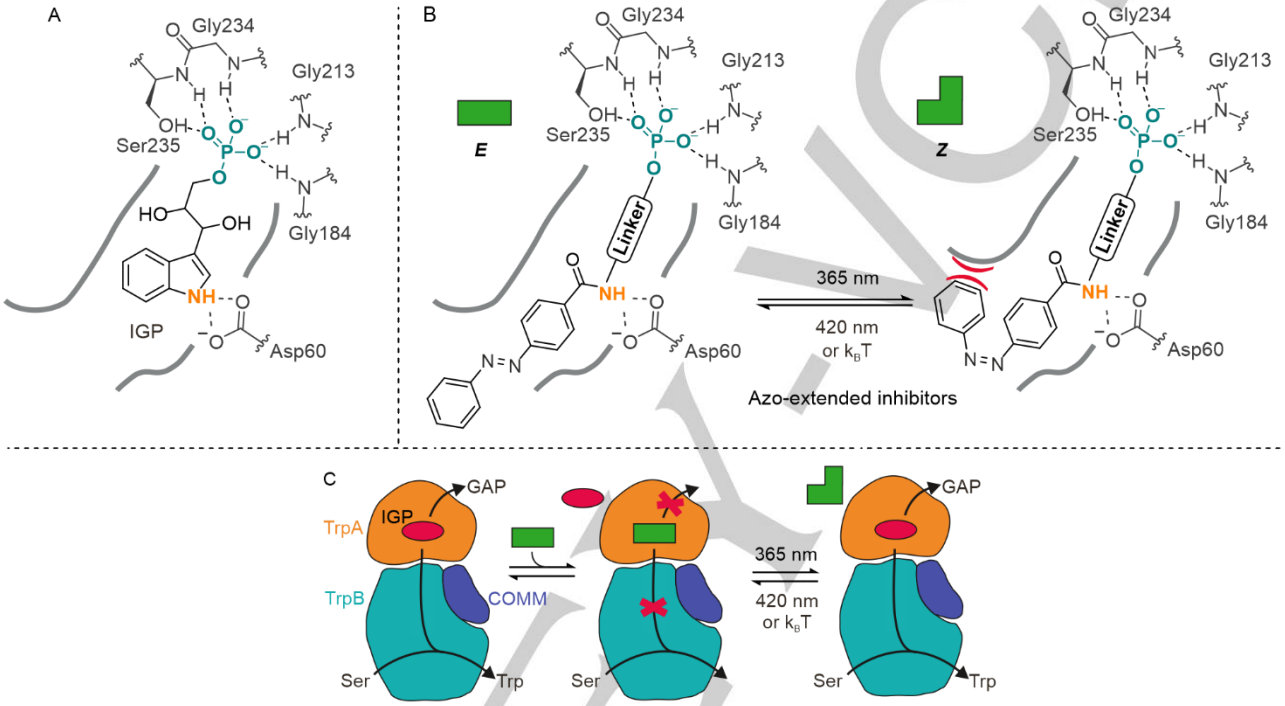

Figure 2. Design of azobenzene inhibitors of TS using the azo-extension approach. **A** Binding of IGP to the active site of TrpA is mainly facilitated by two moieties. The phosphate group (cyan) interacts with the *N*H-groups of the peptide backbone of Gly184, Gly213, Gly234, and Ser235, and with the sidechain of Ser235. The *N*H-group (orange) forms hydrogen bonds to the sidechain of Asp60. Grey lines indicate the dimensions of the binding pocket. **B** The two main binding motifs of IGP, the phosphate and *N*H-group, were integrated in the design of azo-extended TS inhibitors. The phosphate was installed in varying distances to an amide via an aryl or alkyl linker. This biologically active module was then extended with an azo moiety that switches configurations (*E*↔*Z*; indicated by differently shaped green boxes) upon irradiation with UV (365 nm) or visible (420 nm) light. While the *E* isomers are expected to bind similar to the native substrate, steric hinderance between inhibitor and binding pocket (grey) is expected to prevent binding of the *Z* isomers. **C** By displacing IGP (red ellipse) from TrpA with the light-switchable azobenzene inhibitor (green box), TrpA is competitively inhibited and TrpB is deprived of its substrate indole. Upon irradiation with UV light, the *Z* isomer is formed. Due to its higher steric demand, we expect the *Z* isomer to show a lower binding affinity, thus restoring TrpA and TrpB activity. This step is reversed by irradiation with visible light.

Synthesis. For the synthesis of a small library of azobenzene-based inhibitors as defined in our design (Figure 2B), we started from commercially available 4-carboxy azobenzene (**1**, Scheme 1). We converted the carboxylic acid, by treatment with $SOCl_2$, into the corresponding acyl chloride **2**, which was directly reacted with differently functionalized amines to give **3a**–**f** (3–31% yield). As main side reaction, we found chlorination of the arene moiety of the azobenzene as shown by X-Ray analysis in a related work (CCDC-ID 1873980). In the last step, the compounds were reacted with $POCl_3$ using 1,8–bis(dimethylamino)naphthalene (*proton sponge*) as a base to functionalize the alcohol group. Upon aqueous workup, the phosphorus chloride was hydrolyzed, resulting in the corresponding phosphate derivatives **4a**–**f**. After preparative HPLC purification, the compounds were isolated as orange solids. Unreacted starting material as well as losses during the HPLC purification resulted in only low (0.2%) to moderate (37%) yields. Nevertheless, we obtained enough material for photophysical and photochemical studies as well as for a screening of the compounds in a biochemical assay and decided to go on at this stage.

This article is protected by copyright. All rights reserved.

Accepted Manuscript

10.1002/chem.202004061

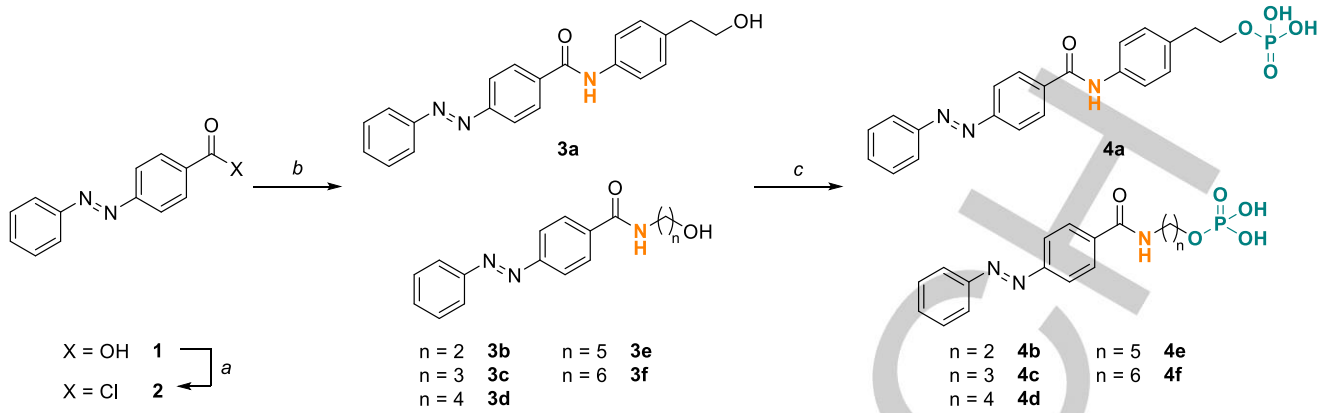

Scheme 1. Synthetic approach towards photochromic TS ligands. *a*: $SOCl_2$, 80 °C, 2 h (not isolated). *b*: 4-(2-hydroxyethyl)aniline or suitable amino alcohol (1 eq), dry pyridine/dry $CHCl_3$ (1:5), r.t., 16 h, 3–31%. *c*: method I: 1) *proton sponge* (3 eq), $POCl_3$, dry THF/dry $CHCl_3$, 0 °C to r.t., 2 h; 2) acetone/water (1:1), 0.2–7% (**4a**,**b**,**d**,**f**); method II: 1) *proton sponge* (3 eq), $POCl_3$, $PO(OMe)_3$, 0 °C to r.t., 2 h; 2) acetone/water (1:1), 0.5–37% (**4c**,**e**).

Photophysical and Photochemical Characterization. We next assessed the solubility and switching properties of our inhibitors in aqueous solution to ensure the compatibility with the buffer system of our target enzyme TS. Compounds **4a,b,d–f** proved to be soluble, and were hence further characterized with UV-visible spectroscopy in water (Figure S5.1.–5.6.); the spectra of **4e** are shown representatively in Figure 3. Spectra were recorded at the thermal equilibrium (black line), after irradiation with UV light of 365 nm (orange line), and after additional irradiation with visible light of 420 nm (green line).

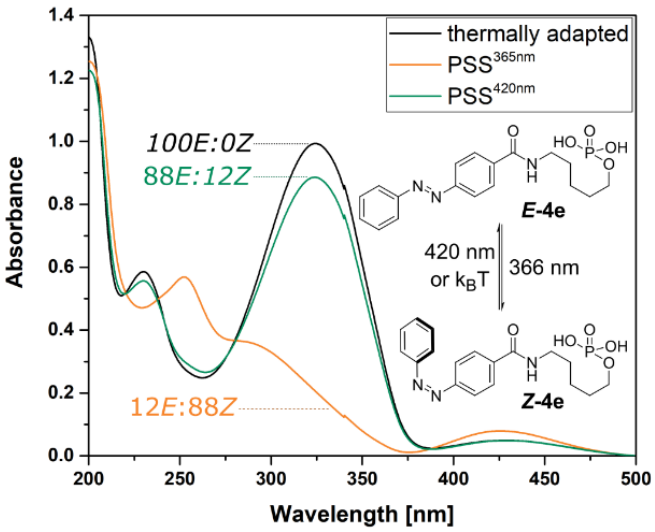

Figure 3. UV-visible spectra of compound **4e** (65 µM) in water. The black line depicts the absorbance spectrum of the azobenzene-based inhibitor at its thermal equilibrium. The orange line represents the photostationary state (PSS) after irradiation with light of 365 nm, and the green line shows the photostationary state after irradiation with light of 420 nm. The photostationary distribution is shown next to each line.

At thermal equilibrium, each compound exhibited a main absorbance maximum between 324 nm and 331 nm (Table 1), which was assigned to the ππ* transition of the *E* isomer.[23] Upon irradiation with light of 365 nm, the photostationary state PSS^{365nm} formed; the signal of the *E* isomer decreased and simultaneously an absorbance maximum between 423 nm and 428 nm emerged, which was attributed to the formation of the nπ* transition of the *Z* isomer. The photostationary state distributions (PSD^{365nm}) were calculated by peak deconvolution with Gaussian functions showing that all compounds accumulated 64–88% of the *Z* isomer. Moreover, the metastable *Z* isomer was found to be sufficiently stable for our measurements (*vide infra*) as we determined a thermal lifetime of 3.76 d for compound **4e** (Figure S5.7.). Subsequent irradiation with visible light of 420 nm induced the photochemical *Z*→*E* isomerization to PSS^{420nm}. However, the composition of the thermal equilibrium could not be fully regenerated—all compounds only accumulated 71–92% of the *E* isomer (PSD^{420nm})—probably due to an overlap of the nπ* band of the *E* and the nπ* band of the *Z* isomer.[23]

Table 1. Overview of photophysical and photochemical properties of compounds **4a,b,d–f** in water.

Compound	λ_{max} (ππ* of *E*)	λ_{max} (nπ* of *Z*)	PSD^{365nm}	PSD^{420nm}
4a	331 nm	423 nm	36*E*:64*Z*	92*E*:8*Z*
4b	324 nm	427 nm	20*E*:80*Z*	71*E*:29*Z*
4d	326 nm	428 nm	21*E*:79*Z*	90*E*:10*Z*
4e	324 nm	427 nm	12*E*:88*Z*	88*E*:12*Z*
4f	325 nm	427 nm	15*E*:85*Z*	84*E*:16*Z*

PSDs were determined by extraction of the PSS by UV−visible spectroscopy via peak deconvolution with Gaussian functions,[27] for details see Figure S5.1.–5.6.

Evaluation of the Inhibition Mode. To analyze the inhibitory potential of our compounds, we first determined the concentration range, in which the azobenzenes inhibited the overall TS reaction (IGP + Ser → Trp + GAP). We measured TS activity by monitoring tryptophan production in a recently established coupled enzymatic assay[24c] in the presence of compounds **4a**,**b**,**d–f** in their *E* or Z (referring to the PSS^{365nm}) configuration. Inhibitor

This article is protected by copyright. All rights reserved.

Accepted Manuscript

10.1002/chem.202004061

concentrations were gradually increased, whereas the IGP and serine concentrations were kept constant at 30 µM (~K_M[24c]) and 5 mM (saturated[24c]), respectively. Compounds **4d–f** showed 30–70% inhibition in the low millimolar range (0.1–0.25 mM, Figure S6.1.). Compounds **4a** and **4b** on the other hand were not able to inhibit TS at soluble concentrations and were therefore excluded from further analyses.

We then quantified the inhibitory effect of compounds **4d–f** in their *E* and *Z* configurations. Since we designed our inhibitors as IGP analogs, we expected a competitive mode of inhibition towards the TrpA substrate (Figure 2C). Hence, we monitored IGP saturation curves for the overall TS reaction in the presence of different inhibitor concentrations. Inhibitor concentrations were chosen from the previous measurements and corresponded to 0% (0 mM), ~30% (0.1 mM), ~50% (0.175 mM), and ~70% (0.25 mM) inhibition. For each IGP saturation curve, an apparent Michaelis constant (K_M^{app}), and an apparent rate constant (k_{cat}^{app}) were determined (Figure S6.2., Table S6.1.). Competitive inhibition is characterized by a decreased K_M^{app} value and an unchanged k_{cat}^{app} value; however, we observed unchanged K_M^{app} values and decreased k_{cat}^{app} values for all our compounds, which indicates that the inhibitors did not compete with IGP for the TrpA active site.

To identify the actual mode of inhibition, we performed global fits using equation 2 (*vide infra*) of the four IGP saturation curves for each inhibitor. By this, we obtained the factor for inhibitor modality α, which indicates the mode of inhibition, and the inhibition constant K_i, which describes the strength of inhibition, for the inhibitors **4d–f** in their *E* and *Z* configurations. All compounds exhibited finite α factors indicative of a non-competitive mode of inhibition[28] (Figure S6.2., Table 2), which confirms our conclusion that the azobenzene inhibitors did not compete with IGP for the TrpA active site. Although the compounds did not follow the intended inhibition mode, they nonetheless revealed K_i values in the low millimolar range (Table 2). In particular, compound **4e** stood out with a K_i of only ~0.18 mM of its *E* isomer and ~0.93 mM of its *Z* isomer, which corresponds to a light regulation factor (LRF) of ~5. In comparison to **4e**, the inhibitory strength of **4d** was 4-fold weaker represented by a higher K_i value, and the LRF of **4f** was 2.5-fold lower. Compound **4e** was consequently chosen as the best candidate for the reversible light-sensitive inhibition of TS as it combines good inhibitory strength with a high potential for light regulation.

We further tested whether the azobenzene inhibitors might associate to the hydrophobic binding site of indole in TrpB instead of the active site of TrpA. Hence, we measured the TrpB reaction (indole + Ser → Trp) with varying concentrations of indole and saturating concentrations of serine, in the presence of our best inhibitor **4e**. The K_M^{app}, k_{cat}^{app}, K_i and α values were determined accordingly (Figure S6.3., Table S6.2.). Similar to the inhibition studies with IGP, the K_M^{app} values remained unchanged, whereas the k_{cat}^{app} values decreased with increasing inhibitor concentrations. Consistently, the α factors for both isomers were finite (~0.7), indicating that compound **4e** does not compete with indole for binding at the TrpB active site. Furthermore, **4e** showed a K_i of ~0.18 mM for its *E* isomer and ~0.50 mM for its *Z* isomer, corresponding to an LRF of ~3, comparable to the measurements with IGP. These results demonstrate that the inhibitory mode of our light-switchable azobenzene inhibitors is also non-competitive towards the TrpB active site.

Table 2. Inhibition values (α, K_i) and light-regulation factors for the IGP- and serine-dependent TS reaction with compounds **4d–f** in their *E* and *Z* configurations.

Compound	Isomer	α	K_i [mM]	LRF[c]
4d	*E*[a]	4.9	0.64 ± 0.08	> 6
	Z[b]	$5.9 \cdot 10^{-5}$	> 4.0	
4e	*E*[a]	0.9	0.18 ± 0.04	5
	Z[b]	0.3	0.93 ± 0.42	
4f	*E*[a]	5.0	0.05 ± 0.00	2
	Z[b]	5.4	0.10 ± 0.01	

[a]*E* refers to the compound at the thermal equilibrium containing ~100% *E* isomer. [b]*Z* refers to the compound with the *Z*-enriched PSD after irradiation with UV light. [c]LRF = light-regulation factor. Values for K_i ± standard error (SE) were determined by fitting the substrate saturation curves for four different inhibitor concentrations (Figure S6.2.) with equation 2 (*vide infra*).

In conclusion, other than originally intended, our synthesized azobenzene-based compounds led to a non-competitive inhibition of TS activity. Nevertheless, inhibition strength could still be light-regulated for all our inhibitors by a factor of 2–6. The *E* configuration conferred a stronger inhibitory effect suggesting that this isomer associates more easily with the TS complex than the sterically more demanding *Z* isomer. Moreover, increasing length of the alkyl linker in **4d–f** resulted in an increasingly stronger inhibition; however, it also reduced the potential for light-responsive inhibition. Our best inhibitor **4e** comprised both, a relatively strong inhibition constant for the *E* isomer of 0.18 mM, and a relatively high LRF. Previously reported TS inhibitors that either bind at the TrpA active site or close to the protein interface showed high or even ultra-high inhibition strengths with K_i values of 4.8 µM[29] and 40 nM[16], respectively. Compared to this, our compound **4e** only reveals a medium strong inhibition strength, which is expected to cause at best a slightly harmful effect on bacteria. However, taking into account that this inhibitor was not designed for a non-competitive inhibition mode, inhibition in the low millimolar range is still noteworthy. We reasoned that by identifying the exact binding site of **4e**, we might be able to optimize the structure of this lead compound, and hence its inhibition strength in future studies.

Co-crystallization of TS with the Azobenzene Inhibitor 4e. For the identification of the binding site of **4e** in the TS complex, we performed co-crystallization experiments. To ensure that TS is uniformly loaded with **4e** in the crystallization set-up, we first determined the binding constant (K_D) of the inhibitor to the TS complex. Isothermal titration calorimetry (ITC) measurements provided a K_D value of ~67 µM indicating a strong binding of **4e** to the TS complex (Figure S7.1.). Additionally, we measured the K_D values of **4e** to the isolated subunits obtaining K_D values of ~130 µM for TrpA and ~10 µM for TrpB, respectively (Figure S7.2., S6.3.). Thus, **4e** binds with a significantly higher affinity to TrpB. We therefore expected that the binding site of **4e** was located in the TrpB subunit. Following this analysis, we crystallized the TS complex in the presence of **4e**—at a saturating concentration (~750 µM) and in excess (~2-fold) over the enzyme—and solved

This article is protected by copyright. All rights reserved.

Accepted Manuscript

10.1002/chem.202004061

its structure (TS_{4e}) with ~2.5 Å resolution (PDB-ID: 7A20; Table S7.1.). The TS_{4e} structure contained two chain pairs of the functional unit of TS per unit cell. Since crystallization took several weeks, we expected to find the *E* isomer instead of the thermally unstable *Z* isomer of **4e** (*vide supra*). However, there was no electron density that could be assigned to the inhibitor. The high binding affinity of **4e** to the TS complex and the high concentrations used for the crystallization experiments led to the conclusion that **4e** was bound to the TS complex but could not be resolved, which suggested highly dynamical behavior of **4e** in the binding site.

We compared TS_{4e} with an active and an inactive conformation of TS to identify potential structural changes induced by **4e** (Figure 4). In the structure of the active TS (TS_{AA}; blue)[13a] an IGP analogue is bound to TrpA, the aminoacrylate intermediate is bound to TrpB, and the COMM domain adopts a "closed" conformation. In the structure of the inactive TS (TS_{IA}; grey)[30] internal aldimine is bound to TrpB, and the COMM domain adopts an "open" conformation. In TS_{4e} (red), no significant structural differences were found in the TrpA subunit and the core structure of the TrpB subunit (Figure 4A). However, the COMM domain is even further shifted towards an "extended-open" conformation (Figure 4B). Notably, the PLP cofactor was missing in the TrpB active site, and instead a single buffer molecule was detected indicating that the TrpB active site is exposed to solvent.

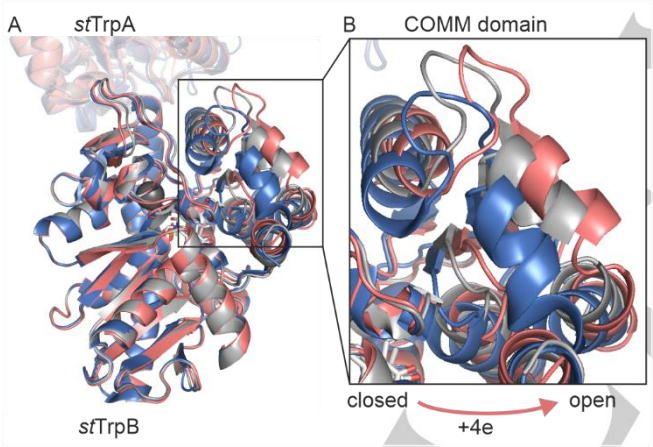

Figure 4. Structural comparison of TS in the presence of **4e** (red; PDB-ID: 7A20, chain pair AB) with the fully active aminoacrylate bound TS_{AA} (blue; PDB-ID: 2J9X, chain pair AB), and the inactive internal aldimine bound TS_{IA} (grey; PDB-ID: 1BKS, chain pair AB). **A** Superposition of the three structures. No structural differences were observed in the TrpA subunit (top, transparent) and the core of the TrpB subunit (bottom). **B 4e** induced significant conformational changes in the COMM domain. While the COMM domain adopts a "closed" conformation in TS_{AA} (blue) and an "open" conformation in TS_{IA} (grey), it is "extended-open" in the presence of **4e** (red).

These findings suggest that **4e** holds the TS complex in an unproductive conformation defined by an "extended-open" COMM domain. Similar observations were made by Arnold and coworkers in their studies on TS from *Pyrococcus furiosus*. They found that a single molecule of β-methyl tryptophan bound to a solvent-accessible binding cleft close to the TrpB active site led to an "extended-open state",[31] meaning that the COMM domain was shifted away from the protein core, similar to our "extended-open" conformation induced by **4e**. This conformation of the COMM domain in TS_{4e} most likely prohibits the allosteric communication between the two active sites and renders both enzymes inactive. In addition, the access to the TrpB active site is opened by the inhibitor so that it is unprotected against the entry of solvent. These effects of **4e** on the TS structure explain the non-competitive mode of inhibition. However, it is still unclear where the binding site of the inhibitor is located and how the inhibitor causes these changes. Since **4e** showed the highest affinity toward the TrpB subunit in binding studies, and since it majorly affected the COMM domain and the TrpB active site in crystallization studies, we continued to search for the binding site in the TrpB subunit by a computational approach.

Computational Analysis of the Putative Inhibitor Binding Site. Even though electron density cannot be detected when a ligand is too dynamical, the binding site can still be traced by identifying pockets in the protein structure that are large enough to accommodate the ligand. Therefore, we analyzed the structures of TS_{AA}, TS_{IA}, and TS_{4e} with the software tool Mole2.5.[32] In TS_{AA}, in which the COMM domain exhibits a closed conformation, no significantly large pockets could be found (Figure S8.1.A). However, in TS_{IA}, in which the COMM domain takes on an open conformation, we identified a surface accessible cavity with a length of ~25 Å located in the cleft between the COMM domain and the TrpB active site (Figure S8.1.B–C). Finally, in TS_{4e}, in which the COMM domain is "extended-open", we also found a cavity at the same location as in TS_{IA} but slightly enlarged with a length of ~29 Å (Figure 5A). This cavity matches the dimensions of the inhibitor (length ~21 Å) and exists in both TrpB chains of TS_{4e} with highly similar size and shape. Binding of our inhibitor to this potential binding site could explain the highly impaired structure of TS_{4e} with the COMM domain in an "extended-open" conformation. Remarkably, β-methyl tryptophan also bound very close to this binding site when inducing the "extended-open state" of TS in previous studies, suggesting that this site might be a novel allosteric binding site of TS.[31] In agreement with this, binding of **4e** led to a non-competitive mode of inhibition with respect to both the TrpA and TrpB active sites. To the best of our knowledge, this binding site has so far been unexplored in inhibition studies. Two other groups described similarly allosteric inhibitors, however, their binding site is located within the indole channel and closer to the TrpA:TrpB interface.[15,16]

Continuing our computational examination, we tested whether **4e** could sterically fit into this cavity and interact with the lining residues. For this, we performed a docking analysis using YASARA.[33] In this experiment, the protein conformation was kept fixed, while the inhibitor was docked with full conformational freedom. As a result, 17 binding geometries could be identified for the inhibitor, out of which ten had predicted K_D values below 5 µM (Table S8.1., Figure S8.2., Figure S8.3.). Remarkably, the orientation of **4e** in most of the binding geometries differed significantly, as illustrated by two exemplary orientations in Figure 5B and 5C, which exhibited predicted K_D values of 0.5 µM and 2.0 µM. In these examples, the phosphate group is either buried at the deep end of the cavity (Figure 5B) or points towards the surface of the protein (Figure 5C). This variety of putative inhibitor geometries in the binding pocket confirms a highly dynamic binding behavior of **4e**, and is therefore consistent with the lack of electron density in the crystal structure.

This article is protected by copyright. All rights reserved.

Accepted Manuscript

10.1002/chem.202004061

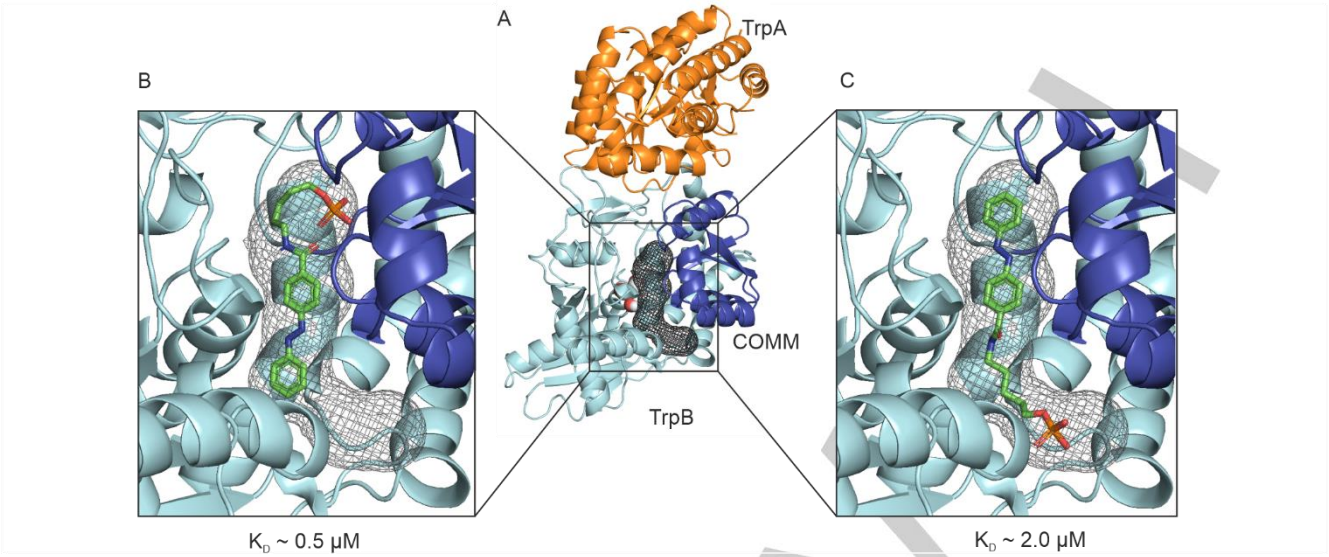

Figure 5. Identification of the **4e** binding site in TS. **A** Mole2.5[32] analysis of TS_{4e} (PDB-ID: 7A20) identified a pocket (grey mesh) between the TrpB active site (marked with the bound buffer molecule in spheres) and the COMM domain (blue) that matches the dimensions of the inhibitor. Note: the cavity is only shown for the chain pair CD however, it also forms in the chain pair AB. **B, C** Docking analysis with YASARA[33] demonstrated that **4e** (green) can bind in various orientations in the in **A** identified binding pocket (black); two variations, which represent the binding orientations of cluster 1 (**B**) and cluster 3 (**C**), are shown with their predicted K_D values.

Photo-Controlling the Non-Competitive Inhibition of TS. Our findings showed that the inhibitor **4e**, which was originally designed to associate at the TrpA active site, most likely binds to a cavity between the TrpB active site and the COMM domain shifting the latter into an unproductive "extended-open" conformation. By this, **4e** might also block the hydrophobic channel, which is located close to its binding site, impeding with the indole transport from the TrpA active site to the TrpB active site. As a result, the light-sensitive inhibition of TS by **4e** is non-competitive. Hence, a revision of our proposed strategy of light-dependent inhibition of TS (Figure 2C) is required.

In the absence of the inhibitor, the allosteric communication between the TrpA and TrpB active sites can take place, activating the turnover of IGP in TrpA and serine in TrpB, respectively (Figure 6A, left panel). The *E* isomer of **4e** binds with high affinity to the TrpB subunit and disturbs the allosteric communication by shifting the COMM domain into the "extended-open" conformation rendering TrpB, and most likely TrpA, inactive (middle panel). As confirmed by inhibition studies, the *Z* isomer, obtained by irradiation with UV light, has a weaker apparent binding affinity and dissociates from the TrpB subunit. Thus, the active, "closed" conformation of the COMM domain is reconstituted, the allosteric communication is restored, and TrpA and TrpB are both reactivated (right panel).

We further evaluated this sequence of events in an *in situ* irradiation setup (Figure 6B). For this, we followed the activity of the overall TS reaction in three samples. One reaction assay was performed in the presence of the inhibitor **4e** in its *E* configuration in the dark ("dark"). The second assay was started in the presence of the inhibitor **4e** in its *E* configuration, and then irradiated during the initial linear activity phase of the enzyme ("direct photo-control"). Moreover, we applied the same treatment as control on a reaction assay in the absence of **4e** ("uninhibited"). TS activity was inhibited ~2-fold by **4e** in the "dark" and "direct photo-control" (prior to irradiation) samples compared to the activity in the "uninhibited" sample. This confirms the medium strong inhibition effect as observed in inhibitory studies and as depicted in the middle panel of Figure 6A. Upon irradiation of the "direct photo-control" sample, the reaction velocity increased 1.2-fold. This LRF is unexpectedly low and disagrees with the LRF determined in K_i studies. However, TS activity in the absence of **4e** in our "uninhibited" sample was 2.2-fold decreased upon irradiation with UV light. We previously observed this effect during our studies on light-control of TS with photo-sensitive unnatural amino acids,[24c] and associated it with a degradation of the light-sensitive PLP cofactor. When we now consider this additional photo-toxic effect, light-induced isomerization of **4e** actually translates into a 2.6-fold regulation of TS activity, approximating the LRF of ~5 in the K_i studies. This recovery of enzyme activity constitutes the situation depicted in the right panel of Figure 6A.

An LRF of 3–5 sets high expectations for the inhibitor's efficacy on bacterial growth. In general, photochromic inhibitors of enzymes are often more convincing *in vivo* than *in vitro*.[17b] This holds true particularly for enzymes in signaling cascades, but also for antibacterial lead compounds, for which it could be shown that an LRF of ~2 is sufficient to control bacterial death with light.[34] The photo-controlled effect of **4e** on the essential multi-enzyme complex TS of *S. typhimurium* is therefore promising, however, various improvements are necessary before its efficacy on bacteria can be proofed and ultimately its antibiotic potential can be tested *in vivo*. First, binding and inhibition strengths need to be increased to improve the effectiveness of the inhibitor in biological systems. For this, the structure of the azobenzene-based compound can be customized for binding to the cavity between the TrpB active site and the COMM domain. Motifs for the specific interaction with residues lining the cavity can be introduced into the linker region or might replace it. Moreover, the wavelength of irradiation needs to be shifted towards higher regions of the electromagnetic spectrum, e.g. in the red region of visible light, to increase the penetration depth of light and minimize photo-toxic

This article is protected by copyright. All rights reserved.

Accepted Manuscript

10.1002/chem.202004061

effects on the tissue. The hazardous effect of UV light was emphasized by the strong decrease of TS activity after irradiation. Optimization of the wavelength of irradiation, but also of the PSD, and the thermal lifetime of the *Z* isomer can be tuned by introducing suitable substituents,[35] or by applying heteroaryl design.[36] Ultimately, the photo-controllable inhibitor can be deployed to tackle common drawbacks of customary antibiotics. These are especially the collateral damage that they cause, for example by attacking pathogenic as well as non-pathogenic bacteria, and their permanent biological activity. As a consequence, accumulation of these drugs in the environment promotes the creation and rapid spreading of multiresistance in bacterial strains.[37] Hence, a spatio-temporally restricted mode of the anti-bacterial efficacy of antibiotics is desirable. Our inhibitor **4e** is not yet suited for this purpose as the less inhibitory *Z* isomer is also the thermally unstable one. Consequently, the amount of the more inhibitory *E* isomer would be increased over time. However, by *e.g.* applying the sign-inversion strategy the thermodynamic stability of the two photoisomers could be inverted rendering the strongly inhibitory *E* isomer the metastable form.[38]

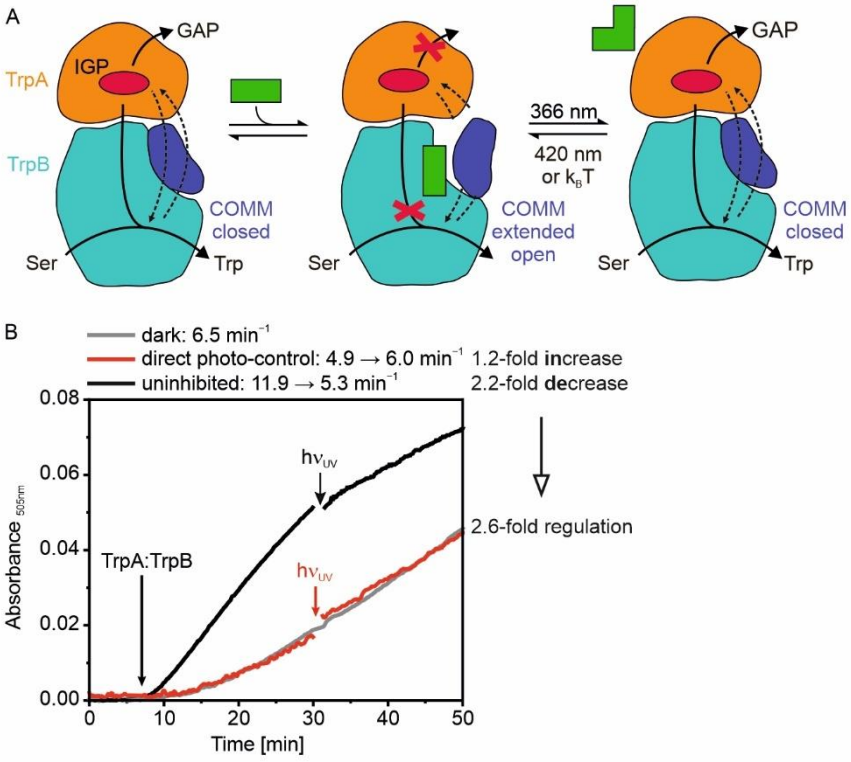

Figure 6. Activity modulation of TS by the photo-switchable non-competitive inhibitor **4e**. **A** Binding of **4e** in its *E* configuration (green rectengular) to TrpB shifts the COMM domain to an "extended-open" conformation, which likely disrupts the allosteric activation between TrpA and TrpB diminishing tryptophan production from IGP (red ellipse) and Ser. Upon irradiation with UV light, the inhibitor is isomerized to its *Z* configuration (green elbow), which restores TrpA and TrpB activity. This step is reversed by irradiation with visible light. **B** Direct photo-control of TS activity with **4e** (red) compared to a "dark" control (kept in the dark; grey) and an "uninhibited" control (in the absence of **4e**, black). Reaction conditions: 50 mM potassium phosphate pH 7.5, 100 mM KCl, 5 mM L–serine, 3.0 mM phenol, 3.0 mM 4–aminoantipyrine, 20 µM PLP, 0.075 g/L HRP, 1.0 g/L VioA and in the case of "direct photo-control" and "dark" 250 µM **4e**. All three reactions were started with the TS complex (0.1 µM), followed for ~30 min, irradiated for 15 s at 365 nm while enzyme velocity was still in the initial linear range, and followed further up to 50 min.

Conclusion

While there is an urgent need, the search for new antibiotics was only recently expanded to inhibitors that target metabolic enzymes or that can be controlled externally. Following this research direction, we set out to explore the TS of *S. typhimurium* as a potential antibiotic target enzyme by designing an inhibitor that can be controlled in a spatio-temporal manner by light. Hence, we synthesized a small library of azobenzene-based inhibitors towards the TrpA subunit. The compounds can be reversibly switched in water up to ~90% of the photochemically generated isomer using UV or blue light, respectively. Inhibition studies quickly identified **4e** as most promising TS inhibitor, as it provides exceptionally good solubility, distinct photochromism, reasonable inhibition and a pronounced difference in inhibition strength between the photo-isomers. This analysis also revealed a non-competitive mode of inhibition towards both the TrpA and TrpB active sites, a finding contrary to our design. We consequently used a combination of ITC-based binding studies, crystallization experiments and computational analyses to unveil the potential binding site of **4e**, a cavity at the TrpB subunit. Moreover, structural analysis showed pronounced conformational changes of the COMM domain, which adopted an allosterically unproductive "extended-open" conformation. In further studies, we aim to improve the design of this new lead compound, taking

This article is protected by copyright. All rights reserved.

Accepted Manuscript

the characteristics of its actual binding site into account, and to optimize the photophysical and photochemical properties of the parent azobenzene. These findings are the starting point to develop fully light-controllable TS inhibitors, which can be further optimized into smart antibiotic agents.

Experimental Section

General Information. Analytical samples of the alcohols and final compounds were purified through preparative HPLC (MeCN in H_2O/0.05% TFA 5-100% over 20 min) to give all compounds as orange solids. NMR spectra were recorded using a Bruker Avance 400 MHz NMR or a Bruker Avance 600 Kryo. Some of the alcohols partly decomposed during the measurement. Thus, carbon signals were assigned using HSQC measurements (quaternary carbons could not be assigned in these cases). Due to the low reaction yields, Carbon NMR was not feasible in case of **4a**-**d**,**f**. A description of the general working methods can be found in section 1. of the Supporting Information.

Synthesis. *General procedure for amide formation*. A crimp top vial was equipped with (*E*)-4-(phenyldiazenyl) benzoic acid (1 eq) and dissolved in $SOCl_2$ (1 mL per 200 mg). The suspension was heated to 80 °C for two hours to give a clear, red solution. The reaction mixture was cooled to ambient temperature and the solvent was removed *in vacuo*. The vial was flushed with vacuum/nitrogen for three times and dry $CHCl_3$ (5 mL) was added under nitrogen atmosphere. To this, a solution of the respective aniline (1 eq) or amino alcohol (1 eq), respectively, in dry pyridine (1 mL) was added dropwise through a syringe. The solution was stirred for 16 h and the solvent was removed *in vacuo*. The crude product was purified through MPLC (20 → 100% EtOAc in petroleum ether).

(E)-N-(4-(2-hydroxyethyl)phenyl)-4-(phenyldiazenyl)benzamide (**3a**). (*E*)-4-(Phenyldiazenyl) benzoic acid (4.42 mmol) was employed. **3a** was obtained in 8 % yield (0.37 mmol). R_f (10%MeOH in DCM): 0.6. ^{1}H NMR (300 MHz, 10% MeOD-*d4* in Chloroform-*d*): δ =8.03 (d, *J* = 8.5 Hz, 2H), 7.98 – 7.93 (m, 2H), 7.92–7.89 (m, 2H), 7.57 (d, *J* = 8.3 Hz, 2H), 7.53 – 7.45 (m, 3H), 7.19 (d, *J* = 8.4 Hz, 2H), 3.76 (t, *J* = 6.9 Hz, 2H), 2.80 (t, *J* = 6.9 Hz, 2H). ^{13}C NMR (151 MHz, Acetone-d_6): δ = 132.0 (+), 130.3 (+), 130.1 (+), 129.6 (+), 123.8 (+), 123.4 (+), 121.1 (+), 64.0 (-), 30.4 (-). Assignment was based on HSQC measurements due to low concentrations and lability of the compound. Thus, quaternary carbons could not be assigned. IR (cm^{-1}) ν= 3351(m), 3045 (w), 2926 (w), 2863 (w), 1648 (s), 1520 (s), 1051 (m), 861 (m), 820 (m), 771 (m), 686 (m). ESI-MS: calculated: 345.1477, found: 713.3 (2MNa$^+$, 5%; 368.1 MNa$^+$, 10%; 346.2 MH$^+$, 100%). HR-MS (ESI): found: 368.1373 (MNa$^+$, 15%), 346.1559 (MH$^+$, 100%).

(E)-N-(2-hydroxyethyl)-4-(phenyldiazenyl)benzamide (**3b**). (*E*)-4-(Phenyldiazenyl) benzoic acid (4.42 mmol) was employed. **3b** was obtained in 31% yield (1.39 mmol). R_f (10%MeOH in DCM): 0.5. ^{1}H NMR (400 MHz, Acetone-d_6) δ =8.10 – 8.05 (m, 2H), 7.98 – 7.90 (m, 4H), 7.60 – 7.51 (m, 3H), 3.68 (t, *J* = 5.7 Hz, 2H), 3.50 (q, *J* = 5.6 Hz, 2H). ^{13}C NMR (151 MHz, Acetone-d_6) δ =129.5 (+), 129.2 (+), 128.2 (+), 122.7 (+), 122.3 (+), 60.8 (-), 42.5 (-). Assignment was based on HSQC measurements due to low concentrations and decomposition of the compound during the extended measuring time. Thus, quaternary carbons could not be assigned. IR (cm^{-1}) ν= 3258 (w), 3064 (w), 3926 (w), 1722 (m), 1626 (m), 1268 (s), 1092 (m), 857 (m), 686 (s). ESI-MS: calculated. ESI-MS: calculated: 269.1164, found: 561.2 (2MNa$^+$, 20%), 292.1 (MNa$^+$, 20%), 270.1 (MH$^+$, 100%). HR-MS (ESI): found: 292.1062 (MNa$^+$, 20%), 270.1242 (MH$^+$, 100%).

(E)-N-(3-hydroxypropyl)-4-(phenyldiazenyl)benzamide (**3c**). (*E*)-4-(Phenyldiazenyl) benzoic acid (2.10 mmol) was employed. **3c** was obtained in 10% yield (0.22 mmol). R_f (10%MeOH in DCM): 0.5. ^{1}H NMR (400 MHz, Acetone-d_6) δ =8.16 – 8.06 (m, 2H), 8.03 – 7.87 (m, 4H), 7.75 – 7.47 (m, 3H), 3.64 (t, *J* = 6.0 Hz, 2H), 3.55 (q, *J* = 6.5 Hz, 2H), 1.80 (p, *J* = 6.3 Hz, 2H). ^{13}C NMR (101 MHz, Acetone-d_6) δ =166.1 (q), 153.9 (q), 152.5 (q), 137.1 (q), 131.7 (+), 129.3 (+), 128.3 (+), 122.8 (+), 122.5 (+), 59.1 (-), 36.9 (-), 32.5 (-). IR (cm^{-1}) ν= 3368 (w), 3291 (m), 3060 (w), 2937 (w), 2881 (w), 1627 (s), 1536 (s), 1073 (m), 775 (m), 686 (s). ESI-MS: calculated: 283.1324, found: 306.1 (MNa$^+$, 20%), 284.1 (MH$^+$, 100%). HR-MS (ESI): found: 306.1215 (MNa$^+$, 20%), 284.1401 (MH$^+$, 100%).

(E)-N-(4-hydroxybutyl)-4-(phenyldiazenyl)benzamide (**3d**). (*E*)-4-(Phenyldiazenyl) benzoic acid (2.21 mmol) was employed. **3d** was obtained in 3% yield (0.06 mmol). R_f (10%MeOH in DCM): 0.5.^{1}H NMR (400 MHz, Acetone-d_6) δ =8.11 – 8.06 (m, 2H), 7.99 – 7.93 (m, 4H), 7.63 – 7.55 (m, 3H), 3.59 (t, *J* = 6.2 Hz, 2H), 3.51 – 3.39 (m, 2H), 1.78 – 1.66 (m, 2H), 1.66 – 1.55 (m, 2H). ^{13}C NMR (101 MHz, Acetone-d_6) δ =165.5 (q), 153.8 (q), 152.5 (q), 137.4 (q), 131.7 (+), 130.8 (+), 129.3 (+), 128.2 (+), 122.8 (+), 122.4 (+), 61.3 (-), 39.6 (-), 30.2 (-), 26.2 (-). IR (cm^{-1}) ν= 3321 (w), 3045 (w), 2926 (w), 2862 (w), 1647 (s), 1521 (s), 861 (m), 820 (s), 771 (s), 865 (s). ESI-MS: calculated: 297.1477, found: 617.3 (MNa$^+$, 40%), 320.1 (MNa$^+$, 20%), 298.2 (MH$^+$, 100%). HR-MS: 320.1376 (MNa$^+$, 40%), 298.1559 (MH$^+$, 100%).

(E)-N-(5-hydroxypentyl)-4-(phenyldiazenyl)benzamide (**3e**). (*E*)-4-(Phenyldiazenyl) benzoic acid (1.33 mmol) was employed. **3e** was obtained in 5% yield (0.07 mmol). R_f (10%MeOH in DCM): 0.8. ^{1}H NMR (400 MHz, Acetone-d_6) ^{1}H NMR (400 MHz, Acetone-d_6) δ =8.11 – 8.05 (m, 2H), 7.99 – 7.94 (m, 4H), 7.63 – 7.56 (m, 3H), 3.54 (t, *J* = 6.3 Hz, 2H), 3.47 – 3.40 (m, 2H), 1.65 (p, *J* = 7.2 Hz, 2H), 1.59 – 1.51 (m, 2H), 1.51 – 1.42 (m, 2H). ^{13}C NMR (151 MHz, Acetone-d_6) δ =130.2 (+), 129.3 (+), 128.2 (+), 122.8 (+), 122.4 (+), 62.3 (-), 40.5 (-), 33.4 (-), 29.4 (-), 24.1 (-). Assignment was based on HSQC measurements due to low concentrations and decomposition of the compound during the extended measuring time. Thus, quaternary carbons could not be assigned. IR (cm^{-1}) ν= 3295 (w), 3052 (w), 2933 (w), 2870 (w), 1714 (s), 1629 (s), 1536 (s), 1271 (s), 1119 (m), 775 (s), 686 (s). ESI-MS: calculated: 311.1634, found: 312.2 (MH$^+$, 100%). HR-MS: 334.1531 (MNa$^+$, 40%), 312.1712 (MH$^+$, 100%).

(E)-N-(6-hydroxyhexyl)-4-(phenyldiazenyl)benzamide (**3f**). (*E*)-4-(Phenyldiazenyl) benzoic acid (4.32 mmol) was employed. **3a** was obtained in 2% yield (0.07 mmol). R_f (10%MeOH in DCM): 0.5. ^{1}H NMR (400 MHz, Acetone-d_6) δ =8.10 – 8.06 (m, 2H), 8.00 – 7.93 (m, 4H), 7.65 – 7.53 (m, 3H), 3.53 (t, *J* = 6.4 Hz, 2H), 3.43 (td, *J* = 7.2, 5.8 Hz, 2H), 1.64 (p, *J* = 7.1 Hz, 2H), 1.56 – 1.48 (m, 2H), 1.45 – 1.36 (m, 4H). ^{13}C NMR (151 MHz, Acetone-d_6) δ 152.8 (+), 152.5 (+), 131.7 (+), 129.3 (+), 128.3 (+), 122.8 (+), 122.4 (+), 62.4 (-), 40.6 (-), 33.8 (-), 30.7 (-), 30.6 (-), 27.2 (-). Assignment was based on HSQC measurements due to low concentrations and decomposition of the compound during the extended measuring time. Thus, quaternary carbons could not be assigned. IR (cm^{-1}) ν= 3384 (w), 3295 (m), 2937 (m), 2855 (m), 1627 (s), 1531 (s), 1297 (m), 858 (m), 775 (s), 686 (s). ESI-MS: calculated: 325.1790, found: 673.3 (2MNa$^+$, 25%), 348.2 (MNa$^+$, 35%), 326.2 (MH$^+$, 100%). HR-MS: 348.1687 (MNa$^+$, 20%), 326.1869 (MH$^+$, 100%).

General procedure I for phosphorylation. An oven-dried crimp top vial was equipped with compound **3a**,**b**,**d**,**f** (1 eq), *proton sponge* (3 eq) and a stirring bar, and sealed. The vial was purged with vacuum/nitrogen (three times each) before dry $CHCl_3$ (1 mL per 0.15 mmol) was added. The reaction mixture was cooled to 0 °C and $POCl_3$ in dry THF (1:2, 0.5 mL per 0.15 mmol) was added dropwise *via* syringe. Then, the mixture was allowed to warm to ambient temperature and was stirred for two hours. After quenching with acetone/water (1:1), the solvent was removed *in vacuo* and the crude product was purified through preparative HPLC (MeCN in H_2O/0.05% TFA, 5→95%). The products were obtained as orange powder after lyophilization.

General procedure II for phosphorylation. An oven-dried crimp top vial was equipped with compound **3c**,**e** (1 eq), *proton sponge* (3 eq) and a stirring bar, and sealed. The vial was purged with vacuum/nitrogen (three times

This article is protected by copyright. All rights reserved.

Accepted Manuscript

10.1002/chem.202004061

each) before $PO(OMe)_3$ (1 mL per 0.15 mmol) was added. The reaction mixture was cooled to 0 °C and $POCl_3$ (0.5 mL per 0.15 mmol) was added dropwise via syringe. Then, the mixture was allowed to warm to ambient temperature and was stirred for two hours. After quenching with acetone/water (1:1), the solvent was removed *in vacuo* and the crude product was purified through preparative HPLC (MeCN in H_2O/0.05% TFA, 5→95%). The products were obtained as orange powders after lyophilization.

(E)-4-(4-(phenyldiazenyl)benzamido)phenethyl dihydrogen phosphate (**4a**). Compound **3a** (125 mg, 0.36 mmol) was employed. **4a** was obtained in 0.5% yield (0.8 mg, 0.002 mmol). HPLC: R_t=15.7 min, >99% purity (220nm), 96% purity (254 nm trace).^{1}H NMR (400 MHz, Methanol-d_4) δ =8.11 (d, *J* = 8.5 Hz, 2H), 8.02 (d, *J* = 8.5 Hz, 2H), 7.96 (dd, *J* = 7.9, 1.9 Hz, 2H), 7.65 (d, *J* = 8.3 Hz, 2H), 7.60–7.54 (m, 3H), 7.30 (d, *J* = 8.4 Hz, 2H), 4.14 (q, *J* = 7.0 Hz, 2H), 2.98 (t, *J* = 7.0 Hz, 2H). ^{31}P NMR (162 MHz, Methanol-d_4) δ =0.00. IR (cm^{-1}) ν= 2922 (w), 2662 (w), 1647 (m), 1524 (m), 1062 (s), 771 (s), 686 (s). ESI-MS: calculated: 425.1141, found: 426.1 (MH^+, 55%), 380.1 (50%), 346.2 (100%), 309.1 (50%), 224.1 (30%); found: 424.1 ($(M-H)^-$, 100%), 344.1 (30%). HR: 426.1210 (MH^+, 100%), 424.1079 ($(M-H)^-$, 100%).

(E)-2-(4-(phenyldiazenyl)benzamido)ethyl dihydrogen phosphate (**4b**). Compound **3b** (374 mg, 1.38 mmol) was employed. **4b** was obtained in 0.2% yield (1.2 mg, 0.003 mmol). ^{1}H NMR (400 MHz, Methanol-d_4) δ=8.07 – 7.89 (m, 6H), 7.62 – 7.48 (m, 6H), 3.79 – 3.69 (m, 4H). ^{31}P NMR (162 MHz, Methanol-d_4) δ=-0.00. ESI-MS: calculated: 349.0828. found: 348.1 ($(M-H)^-$, 100%). IR (cm^{-1}) ν= 3299 (w), 2963 (w), 2930 (w), 1629 (s), 1536 (s), 861 (s), 775 (s), 686 (s).

(E)-3-(4-(phenyldiazenyl)benzamido)propyl dihydrogen phosphate (**4c**). Compound **3c** (63 mg, 0.22 mmol) was employed. **4c** was obtained in 7% yield (5.3 mg, 0.02 mmol). HPLC: R_t= 18.1 min, 95% purity (220 nm and 254 nm). ^{1}H NMR (400 MHz, Methanol-d_4) δ=8.69 (s, 0H), 8.08 – 7.89 (m, 1H), 7.69 – 7.41 (m, 1H), 3.67 (t, *J* = 6.5 Hz, 0H), 3.56 (tt, *J* = 6.9, 2.9 Hz, 0H), 2.10 (p, *J* = 6.7 Hz, 0H). ^{31}P NMR (162 MHz, Methanol-d_4). δ =0.00. IR (cm^{-1}) ν= 3317 (w), 3079 (w), 2937 (w), 2463 (w), 1625 (m), 1543 (m), 1442 (m), 1286 (m), 857 (m), 775 (s), 686 (s). ESI-MS: calculated: 347.3108. found: 346.1 (MH^-, 100%).

(E)-4-(4-(phenyldiazenyl)benzamido)butyl dihydrogen phosphate (**4d**). Compound **3d** (293 mg, 0.99 mmol) was employed. **4d** was obtained in 4% yield (14.7 mg, 0.04 mmol). HPLC: R_t= 18.7 min, 97% purity (220 nm), 95% purity (254 nm). ^{1}H NMR (400 MHz, Methanol-d_4) δ =8.18 – 8.06 (m, 4H), 8.03 – 7.96 (m, 2H), 7.63 – 7.56 (m, 3H), 4.90 (t, *J* = 5.4 Hz, 2H), 3.80 (t, *J* = 6.0 Hz, 2H), 2.46 – 2.32 (m, 2H). ^{31}P NMR (162 MHz, Methanol-d_4) δ =0.00. IR (cm^{-1}) ν= 3414 (w), 3029 (w), 1662 (s), 1275 (m), 1178 (s), 1115 (s), 690 (s). ESI-MS: calculated: 377.1141, found: 378.1 (MH^+, 100%), 247.3 (80%), 223.1 (30%); found: 376.1 ($(M-H)^-$, 100%). HR: 378.1215 (MH^+, 100%), 376.1078 (MH^-, 100%).

(E)-5-(4-(phenyldiazenyl)benzamido)pentyl dihydrogen phosphate (**4e**). Compound **3e** (184mg, 0.59 mmol) was employed. **4e** was obtained in 37% yield (86.7 mg, 0.22 mmol). HPLC: R_t= 13.4 min, 98% purity (220 nm), <99% purity (254 nm). ^{1}H NMR (400 MHz, Methanol-d_4) δ =8.04 – 7.73 (m, 6H), 7.51 – 7.12 (m, 3H), 3.89 (q, *J* = 6.5 Hz, 2H), 3.30 (t, *J* = 7.1 Hz, 2H), 1.70 – 1.48 (m, 4H), 1.40 – 1.28 (m, 2H). ^{13}C NMR (101 MHz, Methanol-d_4) δ =168.0 (q), 154.1 (q), 152.5 (q), 136.4 (q), 131.5 (+), 129.0 (+), 128.0 (+), 122.6 (+), 122.4 (+), 66.2 (-), 39.6 (-), 29.8 (-), 28.6 (-), 22.7 (-).^{31}P NMR (162 MHz, Methanol-d_4) δ =0.16. IR (cm^{-1}) ν= 3313 (w), 3049 (w), 2930 (w), 2860 (w), 1643 (m), 1525 (m), 1010 (s), 771 (s), 686 (s). ESI-MS: calculated: 391.1297, found: 390.1 ($(M-H)^-$, 90%), 269.1 (100%). HR-MS: 392.1372 (MH^+, 100%).

(E)-6-(4-(phenyldiazenyl)benzamido)hexyl dihydrogen phosphate (**4f**). Compound **3f** (24 mg, 0.074 mmol) was employed. **4f** was obtained in 7% yield (1.9 mg, 0.005 mmol). HPLC: R_t= 14.0 min, 95% purity (220 nm), <99% purity (254 nm). ^{1}H NMR (400 MHz, Methanol-d_4) δ =8.02 – 7.92 (m, 6H), 7.60 – 7.51 (m, 3H), 3.97 (q, *J* = 6.6 Hz, 2H), 3.41 (t, *J* = 7.1 Hz, 2H), 1.68 (dp, *J* = 13.7, 6.8 Hz, 4H), 1.46 (dd, *J* = 7.9, 4.4 Hz, 4H). ^{31}P NMR (162 MHz, Methanol-d_4) δ =0.30. IR (cm^{-1}) ν= 3314 (w), 2930 (m), 2855 (m), 1625 (m), 1536 (m), 1014 (s), 775 (s). ESI-MS: calculated: 405.1454, found: 406.2 (MH^+, 25%), 274.3 (100%), 214.1 (90%); found: 404.1 ($(M-H)^-$, 100%). HR: 406.1526 (MH^+, 100%), 404.1388 ($(M-H)^-$, 100%).

Photophysical and Photochemical Characterization. For UV-visible measurements of the absorption spectra of compounds **4a–f** a JASCO V-650 spectrophotometer was used. Compound **4c** and the thermal lifetime of compound **4e** were analyzed using an Agilent 8453 spectrometer. For temperature control, a Varian Cary Single cell peltier apparatus was used. The used solvent and concentration are stated for each experiment. UV-induced isomerizations were performed using a Soul Veasos single-spot LED (365 nm, 0.9 W), an OSRAM Oslon SSL 80 single-spot LED (455 nm, 1.2 W), or a Sylvania UV lamp with two fluorescent black light bulbs with 8 W (settings: 250 mA, 220 V). Sample volume was ≤ 1 mL. For direct photo-control experiments, **4e** was isomerized using a high-power LED (LED Engin, Osram; settings: 700 mA and 16 V) for 15 s. The sample volume was 200 µL.

Bacterial Strains, Plasmids, and Chemicals. The proteins used in this work were produced in the *E. coli* expression strains *E. coli* BL21 Gold (DE3) (purchased from Agilent Technologies, Santa Clara, CA, USA) and *E. coli* BL21 (DE3) Rosetta (purchased from Novagen, Merck, Darmstadt, Germany). The following expression plasmids were taken from previously published work: pET28a_TrpA, pET24a_TrpB and pET28a_VioA.[24c] HRP was purchased from Sigma Aldrich (St. Louis, MO, USA). IGP was produced enzymatically from 1-(o-carboxyphenylamino)-1-deoxyribulose-5-phosphate as described previously.[39] All other chemicals were purchased form commercial sources and were of analytical grade or higher.

Expression and Purification of TS. The genes coding for TrpA and TrpB were heterologously expressed in BL21 (DE3) Rosetta, and BL21 Gold (DE3), respectively. Cells containing expression vectors with the respective genes were grown at 37°C to an OD_{600} of 0.6 in 2–6 L lysogeny broth (LB) medium supplemented with kanamycin. At this point, 0.5 mM IPTG was added to induce gene expression and cells were incubated over night at 20 °C. The cells were harvested by centrifugation, resuspended in 100 mM KP pH 7.5, 300 mM KCl, 20 mM imidazole (20 mL per 1 L cell suspension), and disrupted by sonication. Cell debris and insoluble aggregates were removed by centrifugation. Proteins were purified from the supernatant by nickel-affinity chromatography (HisTrap™ FF Crude column, 5 mL, GE Healthcare) with a linear gradient of imidazole (20 mM→500 mM) followed by size exclusion chromatography (Superdex 75 HiLoad 26/600, GE Healthcare, Chicago, IL, USA) using 100 mM KP pH 7.5, 300 mM KCl as buffer. Fractions containing the purified protein were pooled and dripped into liquid nitrogen for storage at −80 °C.

Expression and Purification of Auxiliary Enzymes. The auxiliary enzyme VioA from *Chromobacterium violaceum* was expressed in BL21 Gold (DE3).[24c] Transformed *E. coli* strains were grown in 4 L lysogeny broth (LB) medium supplemented with kanamycin at 37 °C to an OD_{600} of 0.6. Then, protein expression was induced with 0.5 mM IPTG and cells were incubated overnight at 20 °C. Cells were harvested by centrifugation and the pellets were resuspended in 20 mM Tris·HCl pH 8.0, 300 mM NaCl, and 20 mM imidazole. The target protein was obtained from the supernatant after sonication and repeated centrifugation steps. VioA was captured by nickel-affinity chromatography (HisTrap™ FF Crude column, 5 mL, GE Healthcare, Chicago, IL, USA) and eluted with a linear gradient of imidazole (10→500 mM). Fractions containing the target protein were identified by SDS-PAGE analysis, pooled, and further purified by size-exclusion chromatography (Superdex 75 HiLoad 26/600, GE Healthcare, Chicago, IL, USA) with 20 mM Tris·HCl pH 8.0 as running buffer. Fractions containing the purified protein were pooled and dripped into liquid nitrogen for storage at −80 °C.

This article is protected by copyright. All rights reserved.

Accepted Manuscript

10.1002/chem.202004061

Steady State Activity Measurements and Inhibition Studies. In general, steady state enzyme kinetic measurements were performed at 25°C and followed spectrophotometrically, using a microplate reader (Infinite M200 Pro, TECAN, Männedorf, Switzerland). Turnover of IGP or indole to Trp was measured with a coupled enzymatic assay,[24c] employing VioA, which oxidized Trp producing the side-product peroxide, and horseradish peroxidase (HRP), which then turned over peroxide with 4-aminoantipyrine and phenol to water and a quinone imine. Formation of the latter was followed at 505 nm ($\Delta\varepsilon_{505}$ (quinone imine) = 6,400 $M^{-1}cm^{-1}$).[40] All reactions were started by addition of the TS complex in a 1:1 stoichiometry. Reaction conditions were: 50 mM KP, pH 7.5, 100 mM KCl, 5 mM Ser, 1.0 mM phenol, 1 mM 4-aminoantipyrine, 20 µM PLP, 0.15 g/L HRP, 1.0 g/L VioA, and varying concentrations of substrate (0–200 µM for indole, 0–150 µM for IGP). In order to determine turnover rates, the initial slopes (v_i) of the substrate turnover curves were measured and divided by the total enzyme concentration [E_t]. These turnover rates $v_i/[E_t]$ (in s^{-1}) were plotted against the substrate concentration [S]. Michaelis–Menten constants K_M and turnover numbers k_{cat} were determined by fitting the data with equation 1[28] using Origin 2019 (OriginLab).

$$\frac{v_i}{[E_t]} = \frac{k_{cat}\,[S]}{K_M + [S]} \qquad (1)$$

To identify the concentration range, in which the azobenzenze-based compounds inhibited TS, activity measurements were performed with varying inhibitor concentrations and constant IGP and Ser concentrations. Reaction conditions were: 50 mM KP, pH 7.5, 100 mM KCl, 5 mM Ser, 1.0 mM phenol, 1.0 mM 4–aminoantipyrine, 20 µM PLP, 0.15 g/L HRP, 1.0 g/L VioA, 30 µM IGP and 0–300 mM **4d**–**f**. Reactions were performed at 25 °C. After baseline detection, the reactions were started by addition of the 0.1 µM TS complex in 1:1 TrpA:TrpB stoichiometry. All measurements were performed using a microplate reader (Infinite M200 Pro, TECAN, Männedorf, Switzerland). The initial reaction rates for different inhibitor concentrations were normalized to the reaction rate in the absence of inhibitor, and plotted against the logarithm of the inhibitor concentration.

In order to determine the mode of inhibition, steady-state kinetics were recorded for four different inhibitor concentrations, which correspond to an inhibition of 0% (0 mM), ~30% (100 mM), ~50% (175 mM), and ~70% (250 mM) as measured in the previous set-up. Reaction conditions were: 50 mM KP pH 7.5, 100 mM KCl, 5 mM L–serine, 1.0 mM phenol, 1.0 mM 4–aminoantipyrine, 20 µM PLP, 0.15 g/L HRP, 1.0 g/L VioA and varying concentrations of substrate (0–150 µM for IGP and 0–200 µM for indole). Reactions were started by addition of 0.1 µM TS complex in 1:1 TrpA:TrpB stoichiometry. Fitting the data of a single kinetic experiment to the Michaelis-Menten equation (equation 1) provided an apparent rate constant k_{cat}^{app}, and the apparent Michaelis constant K_M^{app}. The values for the inhibition constant K_i and the α value, which describes the mode of inhibition, were determined using a general model for enzyme inhibition.[28] For this, the steady state kinetic data in presence of inhibitor were evaluated by plotting the measured reaction rates v_i divided by the total enzyme concentration [E_t] against the substrate concentration [S]. The values for k_{cat}, K_M, K_i, and α were determined by a global fit of the four inhibition curves, for the four inhibitor concentrations [I], with equation 2.[28]

$$\frac{v_i}{[E_t]} = \frac{k_{cat}[S]}{[S]\left(1 + \frac{[I]}{\alpha K_i}\right) + K_M\left(1 + \frac{[I]}{K_i}\right)} \qquad (2)$$

Competitive inhibition is characterized by an infinite α value ($\alpha\rightarrow\infty$), because there is no binding of the inhibitor to the enzyme:substrate (ES) complex. Uncompetitive inhibition leads to an α value close to zero ($\alpha<<1$), because there is no binding to the free enzyme.[28] In noncompetitive inhibition, there is affinity for both the ES complex and the free enzyme, which is characterized by a finite value for α.

Determination of Binding Constants. Binding constants were determined by means of ITC measurements using a MicroCal PEAQ-ITC system (Malvern). Solutions of protein (50–100 µM) and **4e** (1.0 mM) were prepared using the same buffer stock (~300 mM Tris/HCl, pH 8.0). Three control experiments, namely the titration of buffer with buffer, the titration of protein solution with buffer, and the titration of buffer with ligand were performed. Each titration experiment was baseline corrected and the signal peaks of each injection were integrated using MicroCal PEAQ-ITC analysis (version 1.22, Malvern Panalytical). Then, each protein-ligand-titration experiment was corrected for each control experiment and processed using the built-in functions of MicroCal PEAQ-ITC analysis with the "single set of identical sites" option. As a result, a ΔH versus molar ratio (ligand:protein) plot and fit values for the binding constant K_D, the number of binding sites *n*, and the molar heat of ligand binding ΔH were obtained. The fitted number of binding sites in initial analyses was close to one. For better comparability, the number of binding sites was then set to one for all experiments.

Crystallization. Tryptophan synthase was co-crystallized with ligand **4e** using the hanging drop vapor diffusion method. For this, TrpA and TrpB were complexed in equimolar amounts and supplemented with a 2-fold excess of ligand **4e** to final concentrations of 30 g/L TS complex and 750 µM ligand **4e** in 50 mM Tris/HCl pH 7.5. 1 µL of the mixture was then mixed with 1 µL of reservoir solution, containing 7% PEG 8000, and 0.1 M sodium citrate, pH 5. Crystals grew within several weeks in a rod-like morphology. Crystals were mounted onto a nylon loop and shock-frozen in liquid nitrogen without addition of further cryoprotectants.

Identification of Tunnels with MOLE 2.5. In order to find cavities within the crystal structure of TS_{4e}, the graphical user interface of MOLE 2.5.17.4.24 was used. The structure of TS_{4e} was loaded into the program and tunnels were identified by applying the automated built in protocol with default parameter settings, i.e. a bottleneck radius of 1.25 Å, an origin radius of 5.00 Å, a surface cover radius of 10.00 Å, a bottleneck length of 0.00 Å, a cutoff ratio of 0.90, a minimum tunnel length of 0.00 Å, and a minimum pore length of 0.00 Å. The default weight function was the Voronoi scale. Note: we use the term "cavity" for the identified pocket, however, Mole 2.5 uses the term "tunnel".

Docking with YASARA. Compound **4e** was docked to TrpB using VINA docking[41] as implemented in YASARA, utilizing the YASARA2 forcefield.[33] For this, TrpB residues 85, 87, 109, 112, 114, 115, 166, 190, 350, 379, and 382 that surround the binding site were set as flexible. Compound **4e** was docked 100 times to different TrpB conformations and the results were sorted according to their estimated binding energy. Additionally, these poses were clustered into 17 distinct complex conformations that had a distance of at least 5 Å deduced as RMSD of the heavy **4e** atoms. Moreover, checking the planarity of the azobenzene moiety after each docking run confirmed that the integrity of the ligand was constantly preserved.

***In Situ* Irradiation.** Reaction conditions for the direct photo-control of enzymatic turnover included 50 mM KP pH 7.5, 100 mM KCl, 5 mM Ser, 1.0 g/L VioA, 0.075 g/L HRP, 100 µM IGP, 1.0 mM 4-aminoantipyrine, 1.0 mM phenole, 20 µM PLP, 200 µM **4e**, and 0.1 µM TS complex. The reaction was started by the addition of the 0.1 µM TS complex in 1:1 stoichiometry and followed at λ = 505 nm with $\Delta\varepsilon_{505}$ (quinone imine) = 6,400 $M^{-1}cm^{-1}$.[40] Measurements were performed in a plate reader (Tecan Infinite M200 Pro) and activities were deduced from the slopes of the transition curves. Altogether two samples and two controls were measured simultaneously. The reaction rate of the first sample was monitored in the dark. The second sample was irradiated during the initial linear activity phase. Control experiments were performed either in absence of **4e** or with buffer instead of TS complex. Irradiation of the second sample and the two controls occurred by pausing the measurement in the plate reader, taking out the plate, and exposing the three wells to UV light, while keeping the other well (positioned furthest away), containing the first sample, covered. The samples were irradiated after 30 min for 15 s with 365 nm (Mouser,

This article is protected by copyright. All rights reserved.

Accepted Manuscript

high power LED, 365 nm, 1.7 V, 700 mA), which corresponded to the irradiation time necessary for *Z*→*E* isomerization under these conditions. The turnover curves of the irradiated second sample and control sample in the absence of **4e** were baseline corrected by subtraction of the buffer control. The first sample was baseline corrected by subtraction of a linear fit of the first 20 min of the buffer control.

Acknowledgements

We thank Elisabeth Bauer, Sonja Fuchs, Jeannette Ueckert, and Sabine Laberer for excellent technical assistance, Stefanie Zwisele for preparing crystals of TS, and Karin Rustler for fruitful discussions. We are grateful to Dr. Stefano Crespi (University of Groningen) for his assistance regarding the PSD analysis. NAS thanks the Studienstiftung des Deutschen Volkes for a PhD scholarship. This work was supported by a grant of the Deutsche Forschungsgemeinschaft to RS (STE 891/12-2).

Keywords: antibiotics • enzymes • inhibitors • photopharmacology • photoswitches

[1] a) M. Tyers, G. D. Wright, *Nat. Rev. Microbiol.* **2019**, *17*, 141–155; b) X. Didelot, K. B. Pouwels, *Nat. Med. (N. Y, NY, U. S.)* **2019**, *25*, 1033–1034;

[2] J. M. Stokes, K. Yang, K. Swanson, W. Jin, A. Cubillos-Ruiz, N. M. Donghia, C. R. MacNair, S. French, L. A. Carfrae, Z. Bloom-Ackermann, V. M. Tran, A. Chiappino-Pepe, A. H. Badran, I. W. Andrews, E. J. Chory, G. M. Church, E. D. Brown, T. S. Jaakkola, R. Barzilay, J. J. Collins, *Cell* **2020**, *180*, 688-702.e13.

[3] D. G. Brown, T. L. May-Dracka, M. M. Gagnon, R. Tommasi, *J. Med. Chem.* **2014**, *57*, 10144–10161.

[4] J. A. Shapiro, A. R. Kaplan, W. M. Wuest, *ChemBioChem* **2019**, *20*, 34–39.

[5] a) I. P. Crawford, *Bacteriol. Rev.* **1975**, *39*, 87–120; b) S. Raboni, S. Bettati, A. Mozzarelli, *Cell. Mol. Life Sci.* **2009**, *66*, 2391–2403;

[6] a) M. F. Dunn, *Arch. Biochem. Biophys.* **2012**, *519*, 154–166; b) C. C. Hyde, S. A. Ahmed, E. A. Padlan, E. W. Miles, D. R. Davies, *J. Biol. Chem.* **1988**, *263*, 17857–17871; c) M. Weyand, I. Schlichting, *Biochemistry* **1999**, *38*, 16469–16480;

[7] W. O. Weischet, K. Kirschner, *Eur. J. Biochem.* **1976**, *65*, 365–373.

[8] M. F. Dunn, V. Aguilar, P. Brzović, W. F. Drewe, K. F. Houben, C. A. Leja, M. Roy, *Biochemistry* **1990**, *29*, 8598–8607.

[9] T. R. M. Barends, T. Domratcheva, V. Kulik, L. Blumenstein, D. Niks, M. F. Dunn, I. Schlichting, *ChemBioChem* **2008**, *9*, 1024–1028.

[10] a) P. S. Brzović, K. Ngo, M. F. Dunn, *Biochemistry* **1992**, *31*, 3831–3839; b) K. Kirschner, A. N. Lane, A. W. Strasser, *Biochemistry* **1991**, *30*, 472–478;

[11] K. S. Anderson, E. W. Miles, K. A. Johnson, *J. Biol. Chem.* **1991**, *266*, 8020–8033.

[12] a) S. Rhee, K. D. Parris, C. C. Hyde, S. A. Ahmed, E. W. Miles, D. R. Davies, *Biochemistry* **1997**, *36*, 7664–7680; b) T. R. Schneider, E. Gerhardt, M. Lee, P. H. Liang, K. S. Anderson, I. Schlichting, *Biochemistry* **1998**, *37*, 5394–5406;

[13] a) H. Ngo, N. Kimmich, R. Harris, D. Niks, L. Blumenstein, V. Kulik, T. R. Barends, I. Schlichting, M. F. Dunn, *Biochemistry* **2007**, *46*, 7740–7753; b) P. Pan, M. F. Dunn, *Biochemistry* **1996**, *35*, 5002–5013; c) M. F. Dunn, D. Niks, H. Ngo, T. R. M. Barends, I. Schlichting, *Trends Biochem. Sci.* **2008**, *33*, 254–264;

[14] a) M. Weyand, I. Schlichting, A. Marabotti, A. Mozzarelli, *J. Biol. Chem.* **2002**, *277*, 10647–10652; b) A. Marabotti, P. Cozzini, A. Mozzarelli, *Biochim. Biophys. Acta* **2000**, *1476*, 287–299; c) A. Sachpatzidis, C. Dealwis, J. B. Lubetsky, P. H. Liang, K. S. Anderson, E. Lolis, *Biochemistry* **1999**, *38*, 12665–12674;

[15] K. A. Abrahams, J. A. G. Cox, K. Fütterer, J. Rullas, F. Ortega-Muro, N. J. Loman, P. J. Moynihan, E. Pérez-Herrán, E. Jiménez, J. Esquivias, D. Barros, L. Ballell, C. Alemparte, G. S. Besra, *Sci. Rep.* **2017**, *7*, 9430.

[16] S. Wellington, P. P. Nag, K. Michalska, S. E. Johnston, R. P. Jedrzejczak, V. K. Kaushik, A. E. Clatworthy, N. Siddiqi, P. McCarren, B. Bajrami, N. I. Maltseva, S. Combs, S. L. Fisher, A. Joachimiak, S. L. Schreiber, D. T. Hung, *Nat. Chem. Biol.* **2017**, *13*, 943–950.

[17] a) M. M. Lerch, M. J. Hansen, G. M. van Dam, W. Szymanski, B. L. Feringa, *Angew. Chem, Int. Ed. Engl.* **2016**, *55*, 10978–10999; b) K. Hüll, J. Morstein, D. Trauner, *Chem. Rev. (Washington, DC, U. S.)* **2018**, *118*, 10710–10747; c) J. Morstein, D. Trauner, *Curr. Opin. Chem. Biol.* **2019**, *50*, 145–151;

[18] a) J. Luo, S. Samanta, M. Convertino, N. V. Dokholyan, A. Deiters, *ChemBioChem* **2018**, *19*, 2178–2185; b) N. L. Mutter, J. Volarić, W. Szymanski, B. L. Feringa, G. Maglia, *J. Am. Chem. Soc.* **2019**, *141*, 14356–14363; c) L. Nevola, M. Varese, A. Martín-Quirós, G. Mari, K. Eckelt, P. Gorostiza, E. Giralt, *ChemMedChem* **2019**, *14*, 100–106;

[19] a) G. M. Murawska, C. Poloni, N. A. Simeth, W. Szymanski, B. L. Feringa, *Chemistry* **2019**, *25*, 4965–4973; b) B. Heinrich, K. Bouazoune, M. Wojcik, U. Bakowsky, O. Vázquez, *Org. Biomol. Chem.* **2019**, *17*, 1827–1833;

[20] a) D. Bliman, J. R. Nilsson, P. Kettunen, J. Andréasson, M. Grøtli, *Sci. Rep.* **2015**, *5*, 13109; b) C. L. Fleming, P. A. Sandoz, T. Inghardt, B. Önfelt, M. Grøtli, J. Andréasson, *Angew. Chem, Int. Ed. Engl.* **2019**, *58*, 15000–15004; c) D. Kolarski, A. Sugiyama, G. Breton, C. Rakers, D. Ono, A. Schulte, F. Tama, K. Itami, W. Szymanski, T. Hirota, B. L. Feringa, *J. Am. Chem. Soc.* **2019**, *141*, 15784–15791; d) X. X. Zhou, L. Z. Fan, P. Li, K. Shen, M. Z. Lin, *Science* **2017**, *355*, 836–842; e) N. N. Mafy, K. Matsuo, S. Hiruma, R. Uehara, N. Tamaoki, *J. Am. Chem. Soc.* **2020**, *142*, 1763–1767;

[21] a) P. Pfaff, K. T. G. Samarasinghe, C. M. Crews, E. M. Carreira, *ACS Cent. Sci.* **2019**, *5*, 1682–1690; b) E. Teichmann, S. Hecht, *ACS Cent. Sci.* **2019**, *5*, 1645–1647;

[22] a) W. A. Velema, J. P. van der Berg, M. J. Hansen, W. Szymanski, A. J. M. Driessen, B. L. Feringa, *Nat. Chem.* **2013**, *5*, 924–928; b) M. Wegener, M. J. Hansen, A. J. M. Driessen, W. Szymanski, B. L. Feringa, *J. Am. Chem. Soc.* **2017**, *139*, 17979–17986;

[23] H. M. D. Bandara, S. C. Burdette, *Chem. Soc. Rev.* **2012**, *41*, 1809–1825.

[24] a) A. C. Kneuttinger, K. Straub, P. Bittner, N. A. Simeth, A. Bruckmann, F. Busch, C. Rajendran, E. Hupfeld, V. H. Wysocki, D. Horinek, B. König, R. Merkl, R. Sterner, *Cell Chem. Biol.* **2019**, *26*, 1501-1514.e9; b) A. C. Kneuttinger, M. Winter, N. A. Simeth, K. Heyn, R. Merkl, B. König, R. Sterner, *ChemBioChem* **2018**; c) A. C. Kneuttinger, S. Zwisele, K. Straub, A. Bruckmann, F. Busch, T. Kinateder, B. Gaim, V. H. Wysocki, R. Merkl, R. Sterner, *Int. J. Mol. Sci.* **2019**, *20*;

[25] A. Fàbrega, J. Vila, *Clin. Microbiol. Rev.* **2013**, *26*, 308–341.

[26] J. Broichhagen, J. A. Frank, D. Trauner, *Acc. Chem. Res.* **2015**, *48*, 1947–1960.

[27] K. Rustler, P. Nitschke, S. Zahnbrecher, J. Zach, S. Crespi, B. König, *J. Org. Chem.* **2020**, *85*, 4079–4088.

[28] R. A. Copeland, *Enzymes*: A practical introduction to structure, mechanism, and data analysis; Wiley-Interscience, Hoboken, NJ, **2000**.

[29] W. O. Weischet, K. Kirschner, *Eur. J. Biochem.* **1976**, *65*, 375–385.

[30] S. Rhee, K. D. Parris, S. A. Ahmed, E. W. Miles, D. R. Davies, *Biochemistry* **1996**, *35*, 4211–4221.

[31] a) A. R. Buller, P. van Roye, J. K. B. Cahn, R. A. Scheele, M. Herger, F. H. Arnold, *J. Am. Chem. Soc.* **2018**, *140*, 7256–7266; b) M. Herger, P. van Roye, D. K. Romney, S. Brinkmann-Chen, A. R. Buller, F. H. Arnold, *J. Am. Chem. Soc.* **2016**, *138*, 8388–8391;

[32] D. Sehnal, R. Svobodová Vařeková, K. Berka, L. Pravda, V. Navrátilová, P. Banáš, C.-M. Ionescu, M. Otyepka, J. Koča, *J. Cheminf.* **2013**, *5*, 39.

[33] E. Krieger, G. Vriend, *Bioinformatics* **2014**, *30*, 2981–2982.

[34] W. A. Velema, M. J. Hansen, M. M. Lerch, A. J. M. Driessen, W. Szymanski, B. L. Feringa, *Bioconjug. Chem.* **2015**, *26*, 2592–2597.

[35] a) D. Bléger, J. Schwarz, A. M. Brouwer, S. Hecht, *J. Am. Chem. Soc.* **2012**, *134*, 20597–20600; b) S. Samanta, A. A. Beharry, O. Sadovski, T. M. McCormick, A. Babalhavaeji, V. Tropepe, G. A. Woolley, *J. Am. Chem. Soc.* **2013**, *135*, 9777–9784;

[36] a) J. Calbo, C. E. Weston, A. J. P. White, H. S. Rzepa, J. Contreras-García, M. J. Fuchter, *J. Am. Chem. Soc.* **2017**, *139*, 1261–1274; b) S. Crespi, N. A. Simeth, B. König, *Nat. Rev. Chem.* **2019**, *3*, 133–146;

This article is protected by copyright. All rights reserved.

Accepted Manuscript

[37] a) D. G. J. Larsson, A. Andremont, J. Bengtsson-Palme, K. K. Brandt, A. M. de Roda Husman, P. Fagerstedt, J. Fick, C.-F. Flach, W. H. Gaze, M. Kuroda, K. Kvint, R. Laxminarayan, C. M. Manaia, K. M. Nielsen, L. Plant, M.-C. Ploy, C. Segovia, P. Simonet, K. Smalla, J. Snape, E. Topp, A. J. van Hengel, D. W. Verner-Jeffreys, M. P. J. Virta, E. M. Wellington, A.-S. Wernersson, *Environ. Int.* **2018**, *117*, 132–138; b) K. Kümmerer, *J. Antimicrob. Chemother.* **2004**, *54*, 311–320;
[38] a) P. Lentes, E. Stadler, F. Röhricht, A. Brahms, J. Gröbner, F. D. Sönnichsen, G. Gescheidt, R. Herges, *J. Am. Chem. Soc.* **2019**, *141*, 13592–13600; b) J. B. Trads, K. Hüll, B. S. Matsuura, L. Laprell, T. Fehrentz, N. Görldt, K. A. Kozek, C. D. Weaver, N. Klöcker, D. M. Barber, D. Trauner, *Angew. Chem, Int. Ed. Engl.* **2019**, *58*, 15421–15428;
[39] S. Schlee, S. Dietrich, T. Kurćon, P. Delaney, N. M. Goodey, R. Sterner, *Biochemistry* **2013**, *52*, 132–142.
[40] M. J. Green, H.A. O. Hill, *Methods Enzymol.* **1984**, *105*, 3–22.
[41] O. Trott, A. J. Olson, *J. Comput. Chem.* **2010**, *31*, 455–461.

WILEY-VCH
Accepted Manuscript

This article is protected by copyright. All rights reserved.

10.1002/chem.202004061

Entry for the Table of Contents

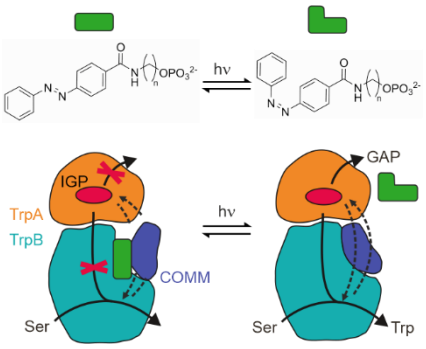

There is growing interest in the spatiotemporal control of drugs for research and medical applications. To this end, we designed a photo-controllable, azobenzene-based inhibitor towards tryptophan synthase, an essential metabolic enzyme complex in bacteria. Thorough biochemical, crystallographic, and computational analyses describe the non-competitive mode of action of this promising antibiotic lead compound.

Institute and/or researcher Twitter usernames: @NadjaSimeth @StratinghInst @univgroningen

WILEY-VCH

Accepted Manuscript

This article is protected by copyright. All rights reserved.